https://doi.org/10.5194/egusphere-2025-5872
Preprint. Discussion started: 4 February 2026

Dynamic drag partitioning in GEOS-Chem (v. 14.2.3) eliminates source function and tuning, revealing equifinality of atmospheric dust observations

Boyan Liu[1], Hongquan Song[1], Adrian Chappell[2], Zhuoli Zhou[2,3]

[1]State Key Laboratory of Spatial Datum, Henan Key Laboratory of Air Pollution Control and Ecological Security, Faculty of Geographical Science and Engineering, Henan University, Zhengzhou, China
[2]School of Earth and Environmental Science, Cardiff University, Cardiff, UK
[3]State Key Laboratory of Earth Surface Processes and Resource Ecology, MOE Engineering Research Center of Desertification and Blown-sand Control, Faculty of Geographical Science, Beijing Normal University, Beijing, China

Corresponding authors: Hongquan Song (hqsong@henu.edu.cn) and Adrian Chappell (ChappellA2@cardiff.ac.uk)

Abstract. Large surface roughness elements (typically vegetation) extract momentum from near-surface winds partitioning it between the vegetation canopy and the unsheltered soil surface, altering the spatial distribution and intensity of dust emission. Data for global drag partition varying over space and time are limited and classical dust models often adopt simplified assumptions or neglect the effect of roughness entirely, relying instead on empirical dust source function to reproduce observed atmospheric dust. Such approaches ignore the three-dimensional spatiotemporal sheltering provided by vegetation and the soil roughness which limits the physical fidelity and predictive capability of dust models. Here we implement the global sheltering parameterization based on surface albedo data in the dust emission scheme of a global atmospheric chemical transport model and evaluate its impact on simulated global dust emissions. We compare simulations from this sheltering parameterization with default settings from classical dust modelling and validate our results against atmospheric dust observations following the widely accepted approach. This is the first study to evaluate the performance of the albedo-based sheltering parameterization globally. The approach eliminates the need for an empirical source function to constrain sources and avoids the need to tune dust emission models. It produces atmospheric dust loadings consistent with atmospheric dust observations despite substantially altering the frequency and spatial pattern of dust emissions. Evidently, different patterns of dust emission frequency can produce similar atmospheric dust loadings, revealing that previous studies intent on reproducing general patterns of large-scale atmospheric dust burden have overlooked the equifinality of dust emission frequency. Accurate dust emission magnitude and frequency remain hampered by entrainment threshold fixed over space, static over time with endless sediment supply, consistent with all other models.

1 Introduction

Dust emission models compute vertical dust fluxes into the atmosphere from the residual wind friction on unsheltered soil particles (Webb et al., 2020). Larger land surface roughness elements such as microtopographic features (soil aggregates, clods,

https://doi.org/10.5194/egusphere-2025-5872
Preprint. Discussion started: 4 February 2026

ripples, rocks, vegetation, etc.) extract momentum from the wind and shelter the soil by reducing the wind friction at the ground and thereby partition drag between the soil bed and larger roughness elements (Shao et al., 2015; Mayaud and Webb, 2017). The drag partition process accounts for the spatio-temporal heterogeneity of sheltering by different scales of roughness which controls both the spatial distribution and intensity of dust emission, therefore making its representation essential for reliable simulation of dust emissions (Webb et al., 2014).

Many parameterizations have been developed to approximate the necessary drag partition processes and the influence of surface roughness elements (Raupach et al., 1993; Marticorena and Bergametti, 1995; Tegen et al., 2002; King et al., 2005; Okin, 2008). However, due to limited data availability on large scale surface roughness, it is difficult to accurately represent the drag partition in global dust emission models (Raupach and Lu, 2004; LeGrand et al., 2023). Consequently, many global dust emission models adopt highly simplified, static assumptions, typically relying on land cover datasets and satellite (green) vegetation products (Klose et al., 2021; Wu et al., 2021), or using globally uniform, empirical parameters (Zender et al., 2003; Gómez Maqueo Anaya et al., 2024). More sophisticated approaches which separate the effect of vegetation and non-vegetation roughness require the values of many parameters which demand extensive ancillary data, limiting their integration into widely used global frameworks. Furthermore, drag partition schemes which are static over time do not represent temporal dynamics or quickly become outdated due to land surface changes e.g., seasonality (vegetation growth), invasive species, wildfires, and land use/land cover change. These changes compound the limitations of drag partitions which fail to represent the complex three-dimensional heterogeneity of landscape roughness elements (Raupach et al., 1993).

These difficulties in adequately representing drag partition are compounded by the long-standing unrealistic assumptions that the entrainment threshold is fixed over space, static over time and with endless sediment, contributing to biases in simulated dust and atmospheric loading and making these models unable to generate reasonable spatial distribution of dust loading directly (without geographical adjustments) (Kok et al., 2014; Leung et al., 2023; Chappell et al., 2023a; Hennen et al., 2024; Shao et al., 2025). Given these model weaknesses (Chappell et al., 2023b), global dust modelling typically 'tunes' the dust emission model results to reproduce the large-scale magnitude and frequency of dust aerosols from satellite or station observed atmospheric dust (Cakmur et al., 2006). For example, dust models often use the fraction of vegetation cover as a mask to exclude dust emissions from vegetated areas (Mahowald et al., 2006; Leung et al., 2023). However, when drag partition is implemented correctly, the sheltering from vegetation already accounts for an additional areal mask is theoretically incorrect and unnecessary (Webb et al., 2020). In this case, the mask geographically adjusts the amount of dust emission, typically to match atmospheric dust observations, often only to North Africa (Huneeus et al., 2011; p.7809). Many other dust model studies use a geographical dust source function (also called an erodibility factor) to confine dust sources across Earth (Ginoux et al., 2004; Fairlie et al., 2007; Meng et al., 2021). These simple restrictions make global dust models reproduce approximately dust loadings which are similar to observations, typically only to North Africa (Huneeus et al., 2011; p.7809). However, most dust source functions are static, not able to represent seasonally changing dust sources in semi-arid regions and interannual variation caused by land cover changes related to human activities. Furthermore, dust source functions determine the intensity of dust emissions based on the observed average state of atmospheric dust. However, dust emissions are fundamentally not the same

https://doi.org/10.5194/egusphere-2025-5872
Preprint. Discussion started: 4 February 2026

as atmospheric dust. Whilst the use of atmospheric dust enables the calibration of dust emission intensity, the approach ignores the frequency of dust events and does little to enable the improvement of dust emission models (Chappell et al., 2023b). Notably, Shao et al. (2025) described in their summary how dust (cycle) models "…commonly constrain the simulated atmospheric dust load using satellite data, but this technique is insufficient to constrain the dust budget, that is, the atmospheric dust load can be forced to agree with the satellite data for the wrong reason". Several studies have suggested that adopting more physically based parameterizations, rather than relying on empirical dust source functions that lack physical processes, could substantially improve the representation of dust emissions (Kok et al., 2014; Li et al., 2022).

Chappell and Webb (2016) proposed a drag partition parameterization that uses albedo (from satellite or ground-based measurements or prognostic estimates) as an integrated proxy for sub-grid scale roughness shadows, thereby directly estimating the fraction of wind stress reaching the soil without needing detailed land cover types. This parametrization has been applied in regional atmospheric and chemical transport model (WRF-Chem) and improved overall magnitude and spatial pattern of dust emissions through better representing dynamic geographic sheltering-effect (LeGrand et al., 2023). This approach describes a simple and efficient drag partition which changes over space and time readily implemented in global dust emission models. Yet, its potential to generate realistic spatial patterns of dust emissions and atmospheric dust loading globally remains untested.

To address this issue, we integrated the physically based albedo drag partition parameterization within the GEOS-Chem framework (version 14.2.3; Bey et al., 2001; Yantosca et al., 2023) to investigate its applicability at the global scale. GEOS-Chem is a three-dimensional chemical transport model that simulates the emission, transport, and mixing of gases and aerosols driven by meteorological inputs from the Goddard Earth Observing System (GEOS) of the NASA Global Modeling and Assimilation Office. GEOS-Chem employs the Dust Entrainment And Deposition (DEAD; Zender et al., 2003) scheme by default as its dust emission scheme. The DEAD model represents wind-driven dust entrainment following the saltation bombardment theory, with a simplified treatment of drag partition. Within GEOS-Chem, a dust source function constrains the spatial distribution of dust emissions produced by the DEAD scheme (Fairlie et al., 2007). This configuration has been widely applied and validated in global dust modelling studies (Johnson et al., 2012; Ridley et al., 2013; Meng et al., 2021; Singh et al., 2024), confirming its robustness and suitability for global-scale simulations. However, several studies have noted that the use of a dust source function can introduce uncertainties in modeled dust concentrations (Tian et al., 2021) and fails to adequately represent the dynamic changes in dust source regions driven by processes such as vegetation dynamics, desertification, and land use/land cover change (Ku and Park, 2013; Song et al., 2024).

We replaced the time-invariant source function used in the DEAD scheme with dynamic drag partition parameterization from albedo data and compared simulations driven by the new albedo parameterization against the standard configuration to assess how drag partition influences both the intensity and frequency of dust emissions across major sources. We evaluated the modelled atmospheric dust against observations following the widely accepted approach to evaluate the global performance of the approach.

https://doi.org/10.5194/egusphere-2025-5872
Preprint. Discussion started: 4 February 2026

2 Methodology

2.1 Dust emission calculation

2.1.1 DEAD scheme in GEOS-Chem

The Goddard Earth Observing System (GEOS) three-dimensional atmospheric chemistry transport model (GEOS-Chem) simulates dust aerosols with diameters below 12 µm and uses the DEAD (Zender et al., 2003) scheme to calculate dust emissions. Total horizontal saltation flux Q_{def} (kg m^{-2} s^{-1}) is calculated based on Kawamura (1951) and later refined by White (1979) using the corrected equation (Sherman et al., 2013):

$$Q_{def} = C_z \frac{\rho}{g} u_*^3 \left(1 - \frac{u_{*t}}{u_*}\right)\left(1 + \frac{u_{*t}}{u_*}\right)^2,\ u_* > u_{*t} \quad , \tag{1}$$

where C_z is a global tuning factor determining the total dust emission strength, ρ is the air density (kg m^{-3}), g is the acceleration of gravity set to 9.8 m s^{-2}, u_* (m s^{-1}) is the above canopy friction velocity and u_{*t} (m s^{-1}) is the soil surface threshold friction velocity. Under natural conditions, where surface roughness causes drag partitioning, it is inappropriate to parameterize sediment transport solely as a function of the above-canopy friction velocity u_*^3 (Webb et al., 2020). Nevertheless, we have retained this default modelling approach for consistency with previous classical dust emission models. In this scheme, dust emission occurs when u_* exceeds u_{*t}, and u_{*t} is influenced by drag partition and soil surface moisture:

$$u_{*t0(D)} = \begin{cases} \left[\frac{0.16666681\rho_p g D}{-1+1.928 Re_{*t}^{0.0922}}\left(1 + \frac{6*10^{-7}}{\rho_p g D^{2.5}}\right)\right]^{1/2}\rho^{-1/2}, & 0.03 \le Re_{*t} \le 10 \\ \left[0.0144\rho_p g D\left(1 - 0.0858 e^{-0.0617(Re_{*t}-10)}\right)\left(1 + \frac{6*10^{-7}}{\rho_p g D^{2.5}}\right)\right]^{1/2}\rho^{-1/2}, & Re_{*t} > 10 \end{cases}, \text{ and} \tag{2}$$

$$u_{*t(D)} = u_{*t0(D)} * f_d * f_w \quad , \tag{3}$$

where $u_{*t0(D)}$ is the threshold friction velocity for smooth and dry soil with particle diameter of D (m), ρ is the air density, and ρ_p is the soil particle density (set to 2650 kg m^{-3}). The threshold friction Reynolds number Re_{*t} is treated as an empirical function of particle diameter D. In the DEAD scheme, D is fixed at 75 µm (75 × 10^{-6} m), representing the optimal saltation diameter (the particle size most easily entrained by wind). The f_d represents the drag partition and f_w considers the effect of surface soil moisture：

$$f_d = \left(1 - \frac{\ln\left(z_{0,m}/z_{0,m}^S\right)}{\ln\left\{0.35\left[\left(0.1/z_{0,m}^S\right)^{0.8}\right]\right\}}\right)^{-1} \quad , \text{ and}$$

(4)

$$f_w = \begin{cases} 1, & w < w_t \\ \sqrt{1 + 1.21\left[100(w - w_t)\right]^{0.68}}, & w > w_t \end{cases} \quad ,$$

(5)

https://doi.org/10.5194/egusphere-2025-5872
Preprint. Discussion started: 4 February 2026

where z_0 is the aerodynamic roughness length above canopy, z_0^s is aerodynamic roughness length of soil surface, w is gravimetric water content, and w_t is the threshold of soil moisture calculated as a function of clay fraction. The DEAD scheme uses values of $z_0 = 100$ µm, $z_0^s = 33.3$ µm and fixes the global distribution of the clay fraction to 0.2 decimal per cent (Zender et al., 2003) which is must larger than clay content in North Africa (Chappell et al., 2023b). However, in the default setup for GEOS-Chem, f_d is set to 1 when applying the source function, which indicates no drag partition is considered. In our simulations, we retained this default setting ($f_d = 1$) when using the source function. In contrast, when the source function was removed, f_d was calculated according to Eq. (4).

The vertical dust flux F_{def} (kg m^{-2} s^{-1}) is considered proportional to Q_{def} using a semi-empirical formulation:

$$F_{def} = f_{erod} S \alpha Q_{def} \quad , \tag{6}$$

where α is the sandblasting mass efficiency, depending on clay fraction (Marticorena and Bergametti, 1995). Since the clay content is fixed to 0.2 in the DEAD scheme, the sandblasting mass efficiency is also globally fixed. The S is the dust source function from the GOCART scheme which reduces dust emissions and restricts them to persistent desert areas based on the geographical distribution of atmospheric dust (Ginoux et al., 2001). The original version of the DEAD scheme does not include this source function and uses vegetation fractions calculated from (green) leaf area index (LAI) data to prevent dust emissions in vegetation covered areas. The f_{erod} is the fraction of erodible land area. It was previously calculated as the reciprocal of the fractions of vertical vegetation cover and snow cover. Fairlie et al. (2007) modified the DEAD scheme in GEOS-Chem to incorporate the dust source function and removed the use of LAI. Therefore, in our modelling with GEOS-Chem, only snow cover is considered (f_{erod} is the reciprocal of snow cover fraction). The F_{def} is divided into four bins to calculate convective transport and dust deposition in the atmospheric module, using the fraction scheme of Zhang et al. (2013).

2.1.2 Drag partition from albedo

In classical dust emission schemes, the drag partition is represented inaccurately by using the total above-canopy u_* directly against the soil surface threshold friction velocity (u_{*t}) to drive sediment transport (Q). In these schemes, the effect of drag partition is accounted for by artificially increasing the threshold friction velocity (by multiplying f_d) rather than by partitioning the total friction velocity (u_*) into surface friction velocity (u_{s*}) which drives sediment transport and dust emission (Webb et al., 2020).

The drag partition parameterization proposed by Chappell and Webb (2016) assumes that shadows from heterogeneous roughness elements can serve as a proxy for the extent of sheltered surface area, which varies with wind speed following Raupach, (1992). The scheme is calibrated using wind tunnel measurements to estimate dust emissions and employs surface albedo data to calibrate drag partition, allowing direct computation of surface friction velocity from wind speed:

$$u_{s*} = u_{ns*} U_f \quad , \tag{7}$$

https://doi.org/10.5194/egusphere-2025-5872
Preprint. Discussion started: 4 February 2026

where u_{s*} is the wind friction velocity at the soil surface, u_{ns*} (also refered to as $\frac{u_{s*}}{U_f}$) is a normalized u_{s*} parameter derived from albedo, and U_f is the wind speed at the freestream height (f), which in this study is set to the standard 10 m above the ground level (LeGrand et al., 2023). The u_{ns*} can be derived from shadow measurements based on an empirical relation:

$$u_{ns*} = 0.0311\left(exp\frac{-\omega_{ns}^{1.131}}{0.016}\right) + 0.007 \quad , \tag{8}$$

where ω_{ns} represents empirically scaled proportion of shadow. To retrieve ω_{ns}, the snow-masked 500 m MODIS albedo product is used to derive normalized shadow proportion (ω_n) as follows:

$$\omega_n = 1 - \frac{\omega_{dir}(0^{\circ})}{f_{iso}} \quad , \tag{9}$$

where $\omega_{dir}(0^{\circ})$ is the daily nadir "black-sky" albedo for MODIS band 1 and f_{iso} is the band 1 isotropic weighting parameter which removes the spectral information leaving only the structural (shadow) information. Then, the ω_{ns} is obtained by scaling ω_n measurements:

$$\omega_{ns} = \frac{(a-b)(\omega_n - 35)}{-35} \quad , \tag{10}$$

where the scaling factors a = 0.0001 and b = 0.01 from Zhou et al. (2024) are used to ensure that ω_{ns} corresponds to the ray-casting results based on reconstructed roughness elements from the wind tunnel study by Marshall (1971).

We use the Google Earth Engine (GEE) to calculate daily ω_{ns} at 500 m across Earth for the year 2016 and then export those data at 50 km resolution. To include ω_{ns} data in the DEAD dust emission scheme within GEOS-Chem, we modified HEMCO (the emission component of GEOS-Chem) to enable new input variables and interpolated daily 50 km ω_{ns} to the same grid domain as our dust emission simulation (0.5° × 0.625°).

In GEOS-Chem, the DEAD scheme retrieves 10 m wind speed from its atmospheric component. Here, u_{s*} is computed following Eq. (7) and Eq. (8). The model derived u_* is then replaced with u_{s*}, and the source function in Eq. (6) is removed, thereby modifying Eq. (1) as:

$$Q_{alb} = C_z\frac{\rho_{air}}{g}u_{s*}^3\left(1 - \frac{u_{*t}}{u_{s*}}\right)\left(1 + \frac{u_{*t}}{u_{s*}}\right)^2, u_{s*} > u_{*t} \quad . \tag{11}$$

Consequently, Eq. (3) is reformulated as:

$$u_{*t(D)} = u_{*t0(D)} * f_w \quad , \tag{12}$$

and Eq. (6) is correspondingly modified to:

$$F_{alb} = f_{erod}\alpha Q_{alb} \quad . \tag{13}$$

Figure 1 shows the computational workflow of the DEAD dust emission scheme before (red) and after (blue) our modification. Detailed descriptions on the implementation are provided in Appendix A. Under this new parametrization, the magnitude and frequency of dust emissions are governed solely by the balance between fixed, static and infinite sediment supply u_{*t} and u_{s*} influenced by varying wind speed and soil surface roughness. Other threshold-related factors, such as soil moisture and soil texture, remain consistent with those in the original DEAD scheme.

https://doi.org/10.5194/egusphere-2025-5872
Preprint. Discussion started: 4 February 2026

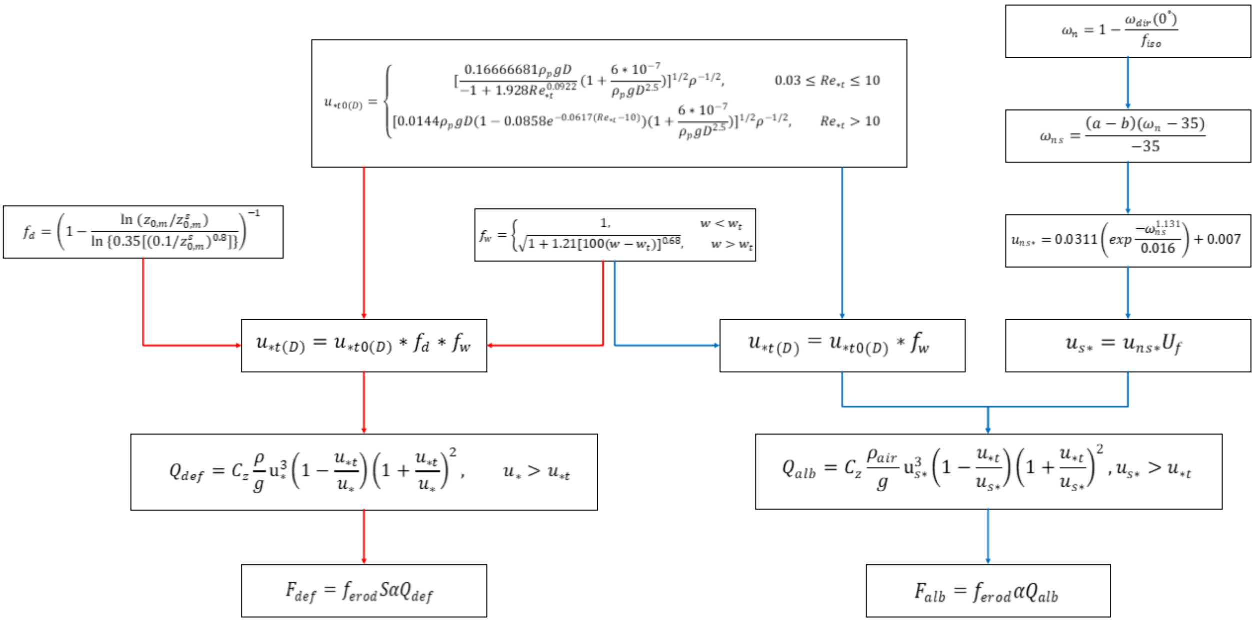

Figure 1: Comparison of the DEAD dust emission scheme in GEOS-Chem between the default configuration (red, with f_d set to 1) and the modified version incorporating the albedo-derived drag partition parameterization (blue).

2.2 Model Configuration

We used GEOS-Chem v14.2.3 to evaluate the performance of different simulation conditions in the DEAD scheme divided between three experiments (Table 1). Experiment 1 (Exp1) uses the default DEAD scheme in GEOS-Chem (with the dust source function, without a drag partition and uses u_* cubed to drive sediment transport). Experiment 2 (Exp2) removes the dust source function and uses simplified drag partition from Zender (2003). Both Exp1 and Exp2 use classical dust emission schemes, and they keep the same u_* cubed to drive sediment transport. The difference between these simulations is that Exp1 sets f_d to 1, and Exp2 sets S to 1, which intend to demonstrate the impact of the simplified drag partition, and how the use of the dust source function impacts dust emissions. Experiment 3 (Exp3) applies the albedo-based drag partition, does not use a dust source function and u_{s*} drives the sediment transport to mobilize dust emission process. For each experiment, we generated dust emissions during 2016, using standalone HEMCO at a global resolution of 0.5° × 0.625°, and then simulated atmospheric dust in GEOS-Chem at a horizontal resolution of 2° × 2.5° with 47 vertical layers. All these schemes were driven by MERRA-2 meteorological data. All simulations were spun up for two months of simulation time to generate suitable background dust concentrations.

https://doi.org/10.5194/egusphere-2025-5872
Preprint. Discussion started: 4 February 2026

Table 1. Experimental configurations for the DEAD dust emission scheme in GEOS-Chem (v14.2.3).

Experiments	Exp1	Exp2	Exp3
Friction velocity	u_*	u_*	u_{s*}
Threshold friction velocity	$u_{*t0(D)} * f_w$	$u_{*t0(D)} * f_w * f_d$	$u_{*t0(D)} * f_w$
Dust source function	S	None	None
Scaling factor	$5.08*10^{-4}$	$1.52*10^{-4}$	$2.38*10^{-4}$

Due to the lack of direct observed global dust emissions (Shinoda et al., 2011; Webb et al., 2016), most global models use atmospheric dust measurements to constrain the magnitude of the global dust budget (e.g., Zender et al., 2003; Tanaka & Chiba, 2006; Ginoux et al., 2012; Meng et al., 2021; Wu et al., 2021; Li et al., 2022; Leung et al., 2023). To simulate reasonable global atmospheric dust loadings and facilitate comparisons between schemes, we followed the approach of Meng et al. (2021) and applied different scaling factors for each simulation to adjust the total annual dust emissions to produce the same outcome of 2000 Tg.

2.3 Datasets

We employ the Land Cover Type Yearly Climate Modeling Grid (CMG) product (Friedl and Sulla-Menashe, 2022) to quantify the proportion of different land cover types and their contributions to total dust emissions. CMG provides sub-grid frequency distribution of land cover classes at a horizontal resolution of 0.05°. We use products based on the International Geosphere-Biosphere Project (IGBP) global vegetation classification scheme and combine 17 IGBP classes into 5 broad categories: barren, grass, shrub, crop, and forest. Fractions of each grid are aggregated into 0.5° × 0.625° resolution for consistency with the GEOS-Chem model. For each grid, the land cover type with the largest proportion is considered as the dominant category. Although uncertainties exist in the IGBP classifications and the model grids are relatively coarse, this approach provides a first-order approximation of dust emissions from different land cover types and facilitates intercomparisons among the three experiments (Table 1).

We use satellite and ground-based observations to validate atmospheric dust simulations, including dust deposition flux, surface dust concentrations, and dust optical depth (DOD). We used dust deposition flux measurements compiled by Albani et al. (2014) from previous publications and datasets for the present-day climate, and these measurements range from several to hundreds of years. Surface dust concentrations originate from the Rosenstiel School of Marine and Atmospheric Science at the University of Miami (Prospero, 1996), compiled monthly (Albani et al., 2014) or using annual averages (Mahowald et al., 2009; Zuidema et al., 2019). These data are mainly measured over a period of two to tens of years. To match the size range in most atmospheric models, Li et al. (2022) applied theoretical or empirical particle-size distributions to convert these deposition and concentration data into multi-year averages for particles smaller than 10 μm. In addition, we compiled PM_{10} measurements from four stations of the Sahelian Dust Transect project (Marticorena et al., 2010) to further complement the validation inventory.

https://doi.org/10.5194/egusphere-2025-5872
Preprint. Discussion started: 4 February 2026

The DOD represents dust distribution in the atmosphere and is typically used for dust model evaluation. Aerosol Robotic Network (AERONET) provides aerosol optical depth (AOD) measurements every 15 minutes (Holben et al., 1998). The AOD at 550 nm are calculated by applying the Ångström exponent α at 440 nm and 870 nm channels combined with AOD at 870 nm. We extracted AOD with $\alpha < 0.75$ to ensure coarse aerosols (mainly dust) dominate, and calculated DOD based on previously established relations between α and fine-mode AOD (Anderson et al., 2005). Stations located over the ocean are excluded to avoid the influence of coarse sea salt aerosols.

We employ the global gridded DOD product provided by Gkikas et al. (2021), except for site observations from AERONET. The MODIS-Aqua dust aeroSol (MIDAS) observation dataset integrates high quality filtered satellite AOD retrievals at swath level (Collection 6.1; Level 2), along with DOD-to-AOD ratios provided by the MERRA-2 reanalysis. This dataset provides continuous, global DOD coverage (which includes the oceans) and complements the AERONET observations, making it suitable for assessing the spatial distribution of atmospheric dust.

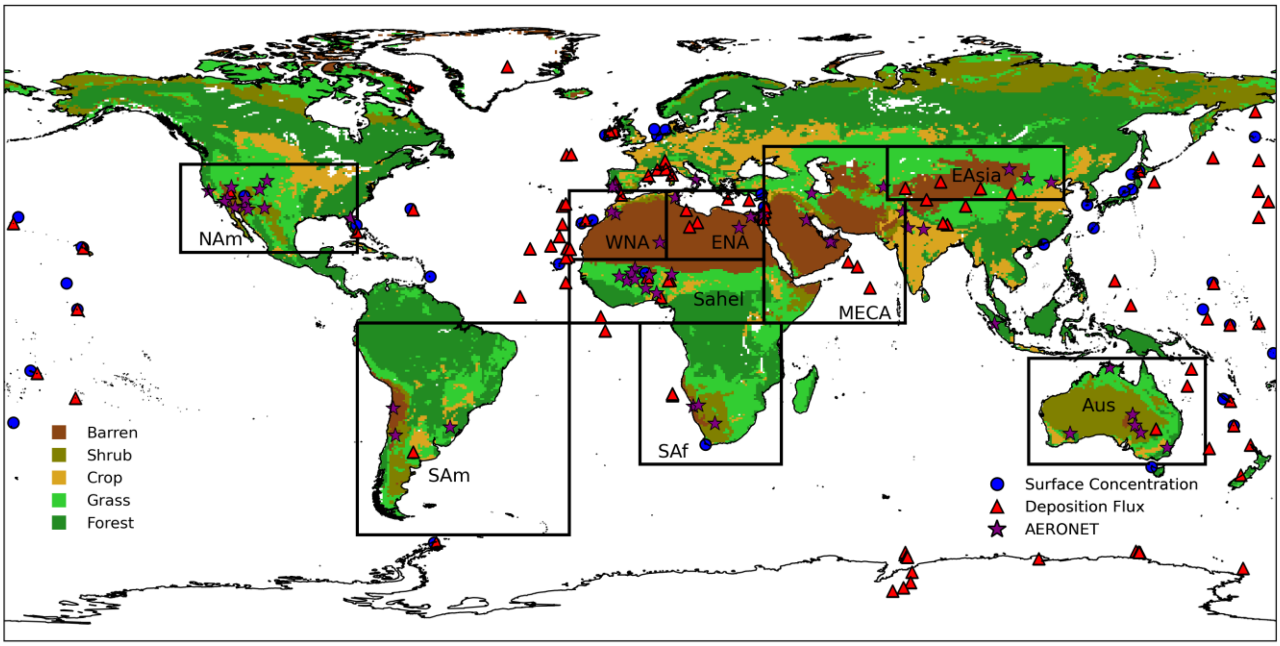

Figure 2: **Spatial distribution of IGBP land cover types, dust observational sites, and major dust source regions following Kok et al., (2021). North Africa is subdivided into West North Africa (WNA), East North Africa (ENA), and the Sahel, while Somalia is included in the Middle East and Central Asia (MECA) source region.**

2.4 Statistical metrics

To compare the seasonality of dust emission across major source regions, we calculate monthly total emitted dust mass and emission frequency. For each grid, we multiply the daily dust emission flux by grid area and seconds per day (86400 s) to obtain daily emitted dust mass and defined a dust emission event as daily emitted mass for each grid exceeding zero. Finally, monthly total emitted dust mass and emission frequency are derived by summing over all grids for each month. Model

https://doi.org/10.5194/egusphere-2025-5872
Preprint. Discussion started: 4 February 2026

performance for the dust cycle is evaluated by comparing simulated annual mean dust deposition fluxes and surface dust concentrations with observations. Scatter plots are drawn using logarithmic coordinates, and statistical metrics are calculated which include the squared correlation coefficient (R^2_{log}) and the mean bias (MB_{log}), both derived from log-transformed values, and the normalised mean bias (NMB), which is calculated from the mean bias divided by mean observations. Although the observational data spans a different time period with our study, it is common to consider the datasets as a climatology for model validation since they cover a long enough period for the present-day climate (Wu et al., 2021). To evaluate the seasonality of atmospheric dust, we calculate multi-year monthly averages and deviations of DOD from AERONET and compare with simulated monthly DOD. Only months with at least 10 days of coarse aerosols dominating observations are retained when computing multi-year averages to minimize the influence of sparse data. For further detailed evaluation, we also compare daily simulated DOD against observations which match the simulation period. For each AERONET station with at least 40 days of coarse aerosols dominating observations in 2016, we calculated the correlation coefficient (R), standard deviation and centred root-mean-square error (CRMSE) between daily modelled and observed values and summarize the results in a Taylor diagram (Taylor, 2001). The Taylor diagram displays three statistics simultaneously: the correlation coefficient is represented by the azimuthal angle (cosine of the angle = R), the standard deviation by the radial distance from the origin, and the CRMSE by the distance from the reference point marked “observed” on the x-axis. Points with coordinates close to the observed coordinates indicate better agreement between model and observations.

3 Results

First, we present the spatial distribution of dust emission flux and contributions from different land cover types. We then compare the seasonality of total dust emissions and dust emission frequency separated into 9 dust source regions (Figure 1). Finally, modelled atmospheric dust are compared with observations to evaluate dust model performance.

3.1 Spatial distribution and seasonality of dust emissions

Figure 3 shows the spatial distribution of modelled annual mean dust emission flux and contributions from different land cover types to total dust emissions in three simulations. All dust emissions are scaled to 2000 Tg, which demonstrates their main differences lie in the spatial distribution of emitted dust. Due to the use of the source function, Exp1 concentrates most dust emissions in barren land and spatial distributions are truncated by the artificial boundaries of the source function. Although other land cover types account for a portion of the dust source area, emitted dust mass from these land cover types contribute little to the total emission because of their smaller weights in the source function. When the source function is removed (Exp2) and the simple drag partition applied, the spatial extent of the dust sources increases. Larger dust contributions occur from all vegetation covered types and notably a large contribution from forests. As previous observational studies (Prospero et al., 2002; Ginoux et al., 2012; Al Nasser et al., 2024) do not show forest as a (major) dust source, this experiment indicates that the simplified drag partition could not generate the correct spatial distribution of dust emissions without the dust source

https://doi.org/10.5194/egusphere-2025-5872
Preprint. Discussion started: 4 February 2026

function. In contrast, Exp3 (without a dust source function) generates a similar spatial pattern of dust sources as Exp1, but with more dust emissions in semi-arid regions including grassland and shrubland in the Sahel, western USA, western Australia, and eastern Inner Mongolia in China. The results demonstrate the importance of an adequate drag partition and suggests that the drag partition from the albedo-based approach restricts the spatial extent of the dust sources without the need for the dust source function.

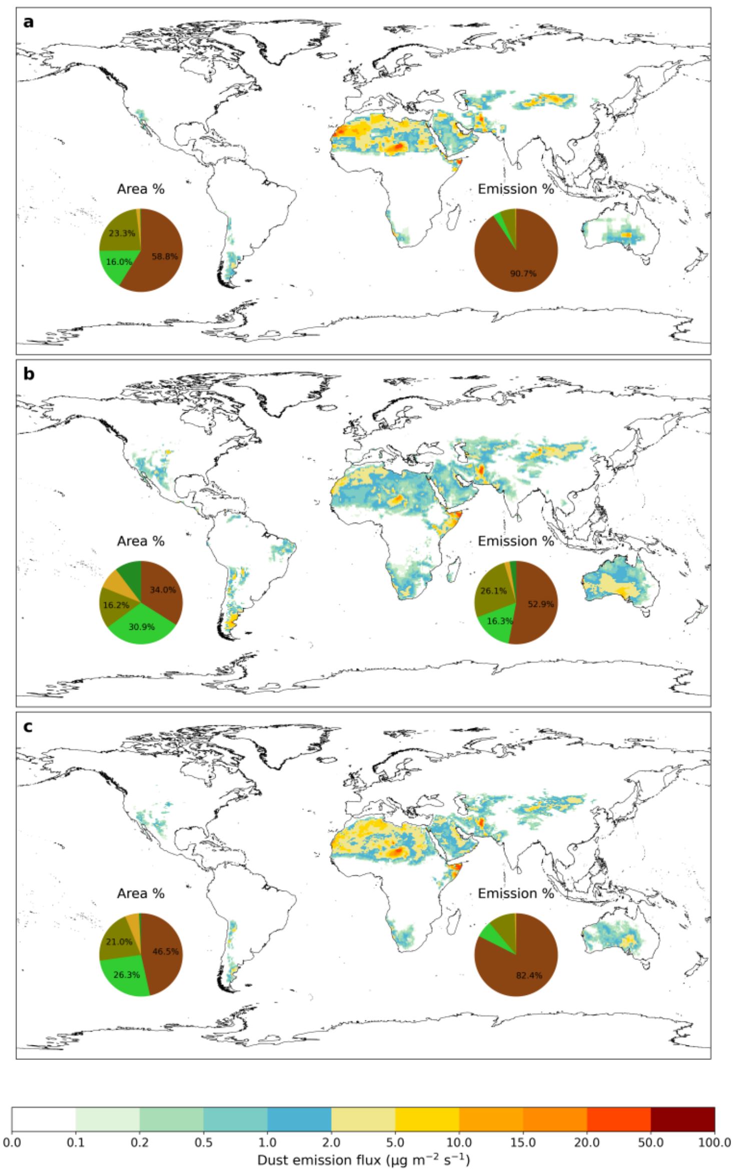

Figure 3: Map showing the spatial distribution of modelled dust emission flux from the three experiments summarised in Table 1: Exp1 (a), Exp2 (b) and Exp3 (c) and pie charts showing the area (%) and emission (%) contributions from the five major IGBP land cover types (Figure 2) using the same legend.

https://doi.org/10.5194/egusphere-2025-5872
Preprint. Discussion started: 4 February 2026

Figure 4 illustrates the seasonal variations in total dust emission mass and dust emission frequency across major dust source regions, highlighting the seasonally shifting dominant dust sources throughout the year. In Exp1 (with dust source function), the dominant dust emission mass region changes from the Sahel in January, to WNA and ENA during February-May, and to the MECA during June-September. During October-December, no single region consistently dominates, although the Sahel and ENA generally show relatively higher emissions. The seasonal pattern of emission frequency differs markedly from that of emission mass, with MECA exhibiting the highest frequency during March-September, and Australia dominating during October-February. In Exp2 (without dust source function), seasonal variations in dust emission mass and frequency remain broadly similar across regions. The Sahel peaks in January-February, MECA in months June-September, and Australia in October-December, while differences among the source regions are relatively minor during remaining months.

Comparisons between Exp1 and Exp2 highlight the impact of applying a source function. While it has little effect on the seasonal pattern of emission frequency, it substantially modifies the magnitude of total dust emissions for different regions. In Exp1, Australia exhibits the highest emission frequency during October-February, whereas the North African regions (WNA, ENA, and Sahel) never peak in frequency throughout the year. However, the source function suppresses dust emission mass in Australia and enhances it in North Africa. Consequently, North African sources dominate the total emission mass during January-May, whereas emissions from Australia remain consistently small throughout the year. In contrast, the use of u_{s*} not only change the magnitude of emitted dust mass but makes a difference to the emission frequency.

Exp3 (without a dust source function) produces a seasonality of emitted dust mass like Exp1. Both simulations produce larger emission mass in WNA and ENA than other dust sources during March-May and produce no peak in Australia during October-December. However, the two experiments show very different emission frequency. In general, Exp1 indicates more dust emission events than Exp3 due to the absent drag partition, indicating that Exp1 tends to generate consistently small intensity dust emissions due to the use of the dust source function. In contrast, Exp3 tends to produce fewer dust events with relatively strong intensity. Exp3 also shows a consistent seasonal pattern between emission mass and frequency among regions, with higher emission frequency in North Africa during March-May and lower frequency in Australia during October-February. This consistency is absent in Exp1 because the source function decouples emission mass from frequency.

https://doi.org/10.5194/egusphere-2025-5872
Preprint. Discussion started: 4 February 2026

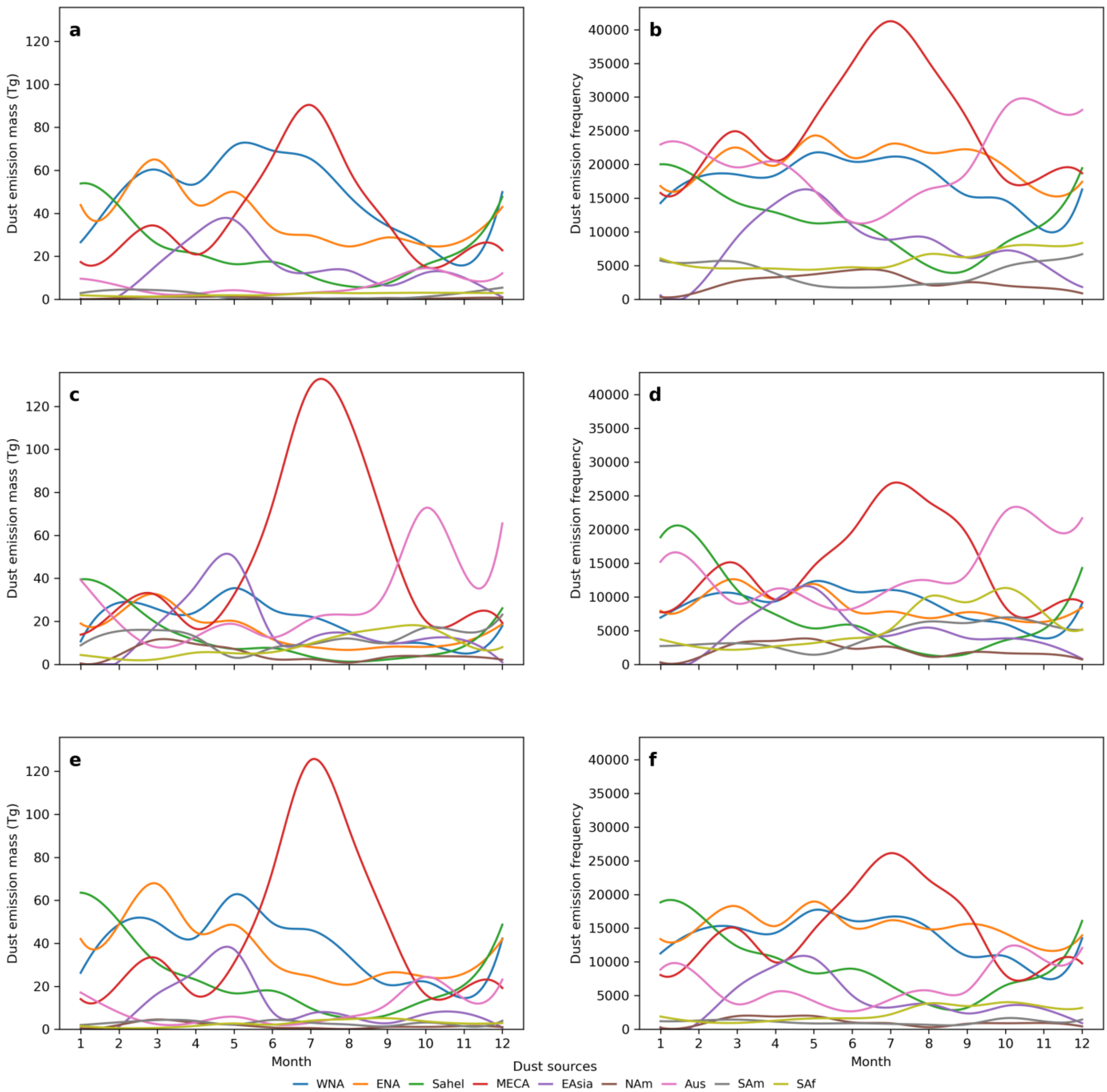

315

Figure 4: Modelled monthly total dust emissions (left column) and dust emission frequency (right column) for different dust source regions under different simulation conditions (Table 1): Exp1 (a & b), Exp2 (c & d) and Exp3 (e & f).

Overall, the absence of a drag partition (Exp 1) or simplified drag partition (Exp 2), cause these simulations to fail to reproduce a reasonable spatial distribution of dust emissions (in Exp 2) and therefore require a source function to tune emitted dust mass

https://doi.org/10.5194/egusphere-2025-5872
Preprint. Discussion started: 4 February 2026

for different regions (in Exp 1). Unfortunately, the use of the source function hardly alters the emission frequency, revealing inconsistency with emitted dust mass.

3.2 Model validation against atmospheric dust cycle

Figure 5 compares the simulated annual average DOD with MODIS observed DOD. Two simulations (Exp1 and Exp3) reproduce the strong dust burden over North Africa, the Middle East and East Asia. In contrast, Exp 2 does not produce those same strong dust burdens and produces excessively large DOD over Australia and over large areas without strong dust sources including North America, South America and Southern Africa, compared with observations. This difference indicates that the classical dust model requires the source function to tune the spatial distribution of dust emissions to reproduce observed atmospheric dust burdens. In contrast, the albedo-based dust model does not require a prescribed source function, its drag partition adequately reproduces the geographical distribution and dust burden of MODIS DOD.

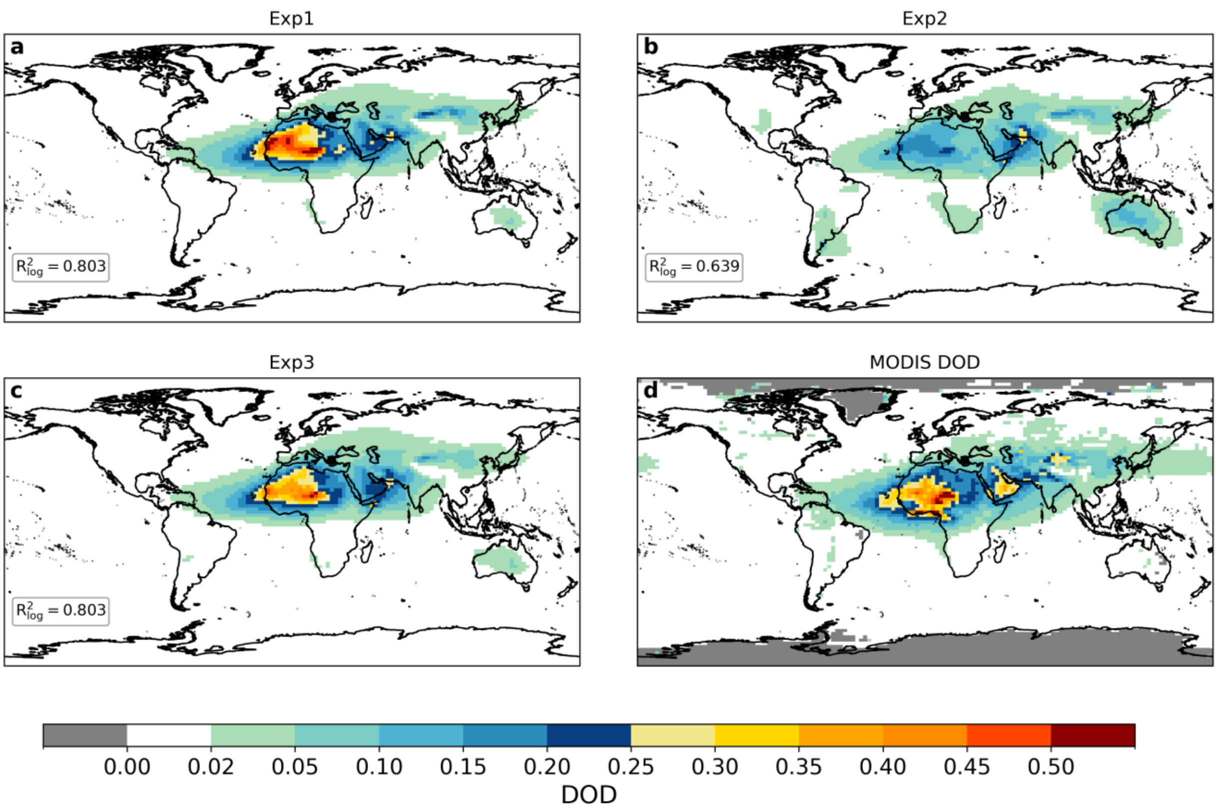

Figure 5: Annual mean dust optical depth (DOD) in 2016 for Exp1 (a; with dust source function), Exp2 (b; without dust source function), and Exp3 (c; albedo-based drag partition) (Table 1), and MODIS observations (d).

Figure 6 presents the seasonality of DOD measured and modelled (Exp1, Exp2 and Exp3) at stations selected with the most complete year-round records and broad spatial coverage. At most sites, Exp1 and Exp3 produce similar performance and

https://doi.org/10.5194/egusphere-2025-5872
Preprint. Discussion started: 4 February 2026

represent the main observed seasonal variations of atmospheric dust. In contrast, the results of Exp 2 are rarely like the results of the other experiments and the observations.

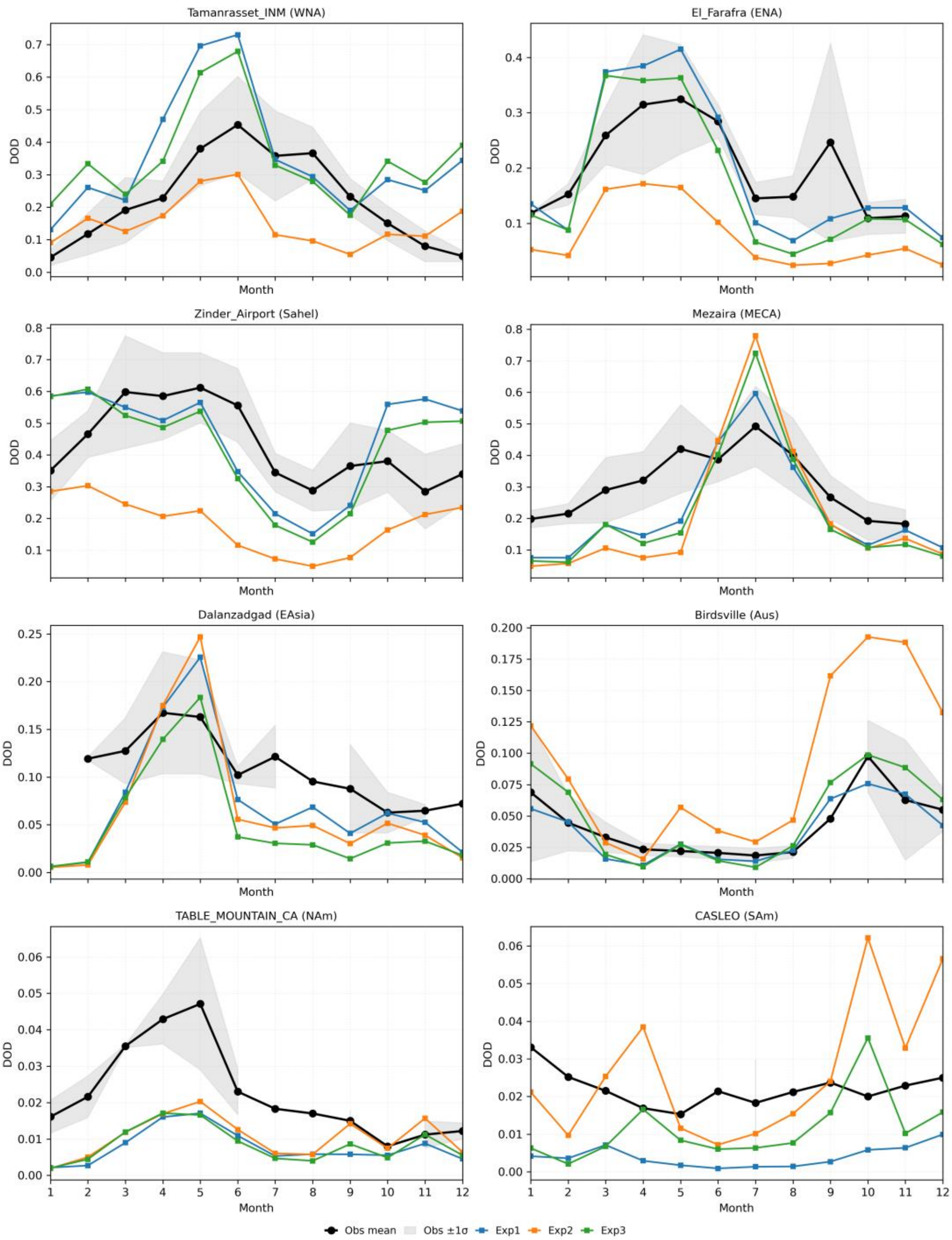

340 **Figure 6: Monthly mean dust optical depth (DOD) from Exp1 (with dust source function), Exp2 (without dust source function), and Exp3 (albedo-based drag partition) compared with AERONET observations.**

Figure 7 uses the Taylor diagram (Taylor, 2001) to summarise daily averaged DOD statistics during the 2016 simulation period, with the standard deviation in the radial coordinates and the correlation coefficient (*R*) in the azimuthal position. Better model performance is indicated by points closer to the observed marker. Among all experiments, *R* is largest in North Africa and smallest in North America and Australia. Exp2 shows inflated standard deviations at sites in South Africa, North America, and Australia, while underestimating variability in North Africa. Exp1 and Exp3 still perform similarly, with their standard deviations close to observations among most sites in North Africa, South Africa and the Middle East. The main difference between these experiments is that Exp1 overestimates the standard deviation at several sites in East Asia, Australia and North Africa, while Exp3 improves its standard deviation, resulting in better overall CRMSE but without a clear improvement in correlation. Overall, the albedo-based drag partition without a dust source function enables the dust model to perform similarly to the classical dust model using the source function.

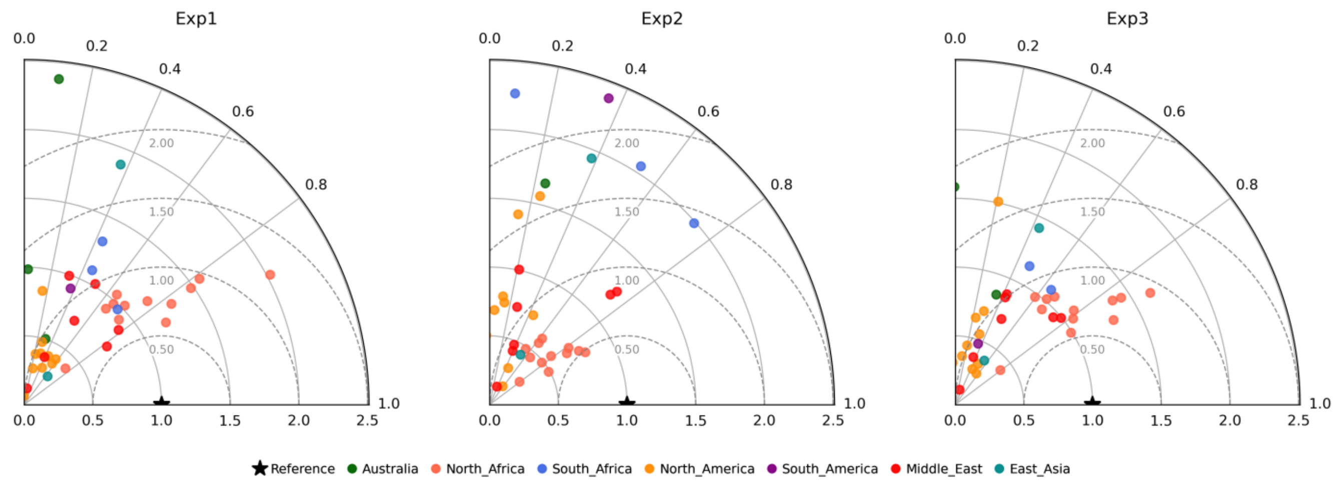

Figure 7: Taylor diagram displaying the correlation (*R*) along the arc and the standard deviation along the x-axis to describe model performance compared with measurements of dust optical depth (DOD) colour coded for the different dust source regions showing the results for each experiment (Table 1) Exp1 (with dust source function), Exp2 (without dust source function), and Exp3 (albedo-based drag partition).

Figure 8 compares modelled surface dust concentrations and dust deposition fluxes with site observations. Observed surface dust concentrations at 40 sites span roughly 10^{-2}-10^{2} µg m^{-3}, while 108 deposition sites span roughly 10^{-3}-10^{2} g m^{-2} yr^{-1}, indicating large spatial variability in dust concentration and deposition. For surface concentration, all simulations (Exp1, Exp2 and Exp3) correlations with observations are relatively strong ($0.73<R^2_{log}<0.79$). More than 90% of the sites show model biases within 10 times (red dashed lines) of the 1:1 line (black dashed line). For deposition flux, all simulations (Exp1, Exp2, and Exp3) show weaker correlations ($0.48<R^2_{log}<0.60$) than the surface concentrations and ore sites have biases beyond the 10 times lines. Simulations Exp1 and Exp3 yield similar correlation coefficients with observations (0.79/0.78 and 0.60/0.58, respectively), and both Exp1 and Exp3 simulation correlation are larger than Exp2 correlations with observations (0.73 and 0.48). Compared with simulated DOD, dust concentrations and deposition flux show larger discrepancies because most of

https://doi.org/10.5194/egusphere-2025-5872
Preprint. Discussion started: 4 February 2026

these observational sites are located far from dust sources, which makes them less directly related to dust emission and more sensitive to model transport and deposition processes.

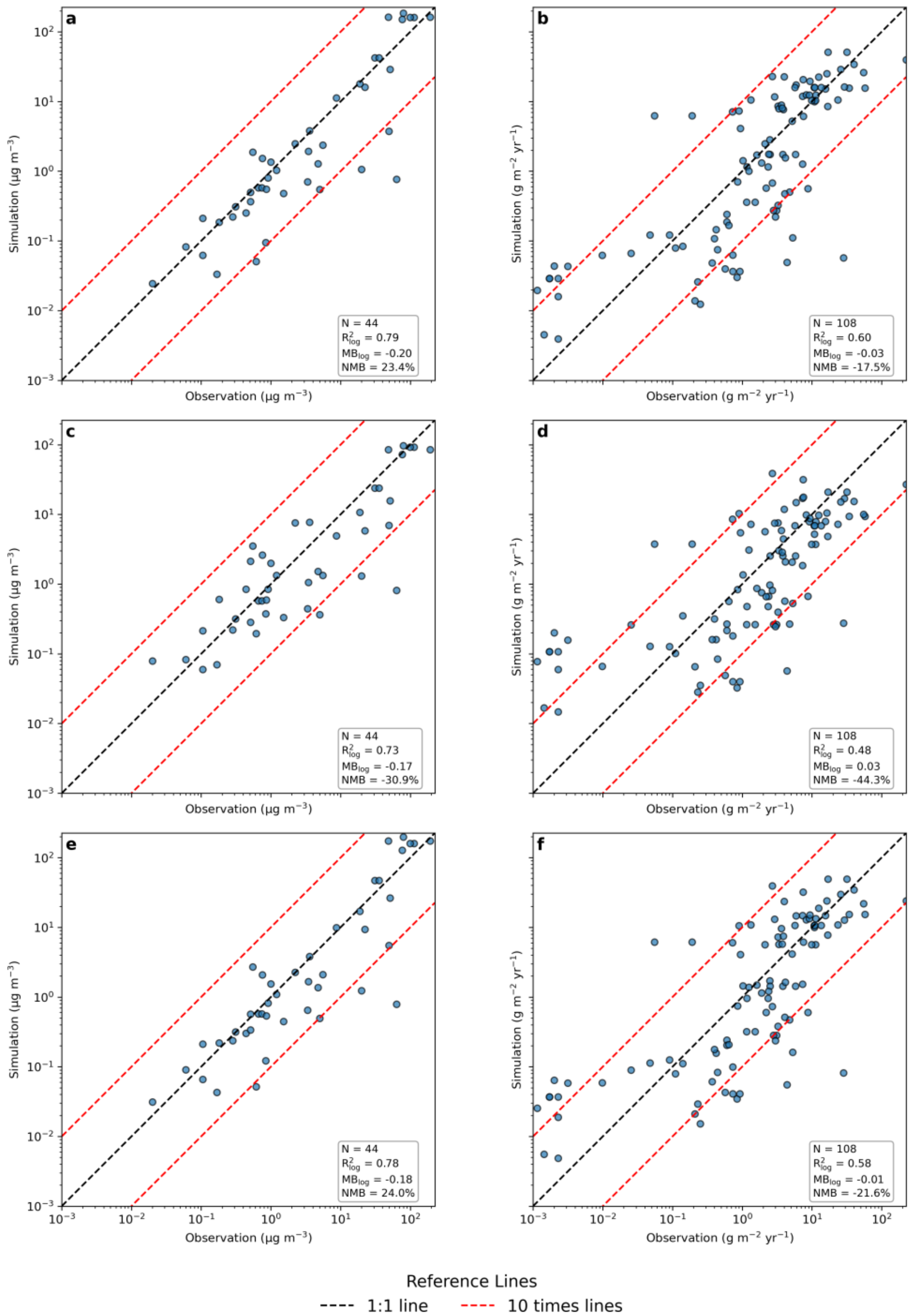

370 **Figure 8: Scatterplots of surface dust (particulate matter < 10 μm; PM_{10}) concentration (left column) and dust deposition flux (right column) from three experiments (Table 1) Exp1 (a and b), Exp2 (c and d), and Exp3 (e and f).**

https://doi.org/10.5194/egusphere-2025-5872
Preprint. Discussion started: 4 February 2026

4 Discussions

Results from our experiments show that the truly dynamic drag partition from the albedo-based parameterization achieves a similar outcome to the longstanding use of a simplified drag partition combined with a fixed over space and static over time dust source function. This albedo-based parameterization significantly improves the simulation of global dust emission relative to classical models which overestimate the extent of dust sources and depend on the (fixed and static) constraints from the dust source function. Although providing a more sophisticated representation of the drag partition, one which changes with wind speed, the albedo-based parameterization provides a suitable balance between fidelity of process and parsimony in implementation (Raupach and Lu, 2004) making the parameterisation ideal for large scale dust modelling. This albedo-based parameterization alters the frequency of emitted dust, relative to that using the dust source function but comparisons with observed atmospheric dust do not show any improvement. We interpret these results to mean that atmospheric dust observations are not diagnostic of the dust emission model performance. We think there are at least two main causes for this mismatch between improved dust emission model performance and limited difference in atmospheric dust observations:

1. Coarse resolution of the chemical transport model. We simulate the transport and deposition of dust aerosols in a horizontal resolution of $2^{\circ} \times 2.5^{\circ}$, which hinders the ability to resolve localized, short-lived emission events that are captured by station measurements. At such large grid spacing, narrow plumes and transient sources are smoothed and diluted by advection and mixing. Furthermore, and beyond the scope of this study, these models are not parameterised to scale linearly and consequently, the inherent sub-grid scale heterogeneity is not adequately represented (Chappell et al., 2024).
2. Atmospheric dust accumulation. Two of our experiments (Exp1 and Exp3) differ markedly in monthly emission frequency (Figure 4). However, the variation and magnitude of DOD (Figure 6) change little. This is because dust emissions and atmospheric dust are only partially connected, and atmospheric dust is also strongly related to model transport. Emitted dust persists and accumulates in the atmosphere, and DOD represents the total atmospheric dust load accumulated prior to the observation rather than instantaneous dust emissions. Consequently, DOD is relatively insensitive to changes in the frequency of emitted dust. For example, multiple low-intensity dust emissions can produce a similar atmospheric dust load to one single high-intensity event. There is an inherent equifinality (many possible combinations can produce the same outcome) in using accumulated sediment. This is well known in geomorphology (Beven, 2006), dating back to at least river suspended sediment and mixture modelling in the 1970s (Walling, 1977). This interpretation implies that previous dust model evaluation and calibration approaches that only rely on atmospheric dust observation are very likely to have over-estimated the performance of dust models in reproducing the timing and occurrence of dust emission events.

It is important to recognise that there remain gross simplifications in the dust emission model. These model simplifications are longstanding and consequently very well-known but are persistently overlooked when comparing dust emission model results to the atmospheric dust observations. These simplifications include the threshold friction velocity which is fixed over space

https://doi.org/10.5194/egusphere-2025-5872
Preprint. Discussion started: 4 February 2026

(within soil texture classes) and static over time, and which assumes an endless supply of sediment transport. This last aspect has recently been shown to have a profound impact on the dust results (Shao et al., 2025). Specifically, the DEAD scheme adopts the threshold for particles with a diameter of 75 μm as the minimum threshold for each grid cell. However, soils are not mobilized independently, and the threshold for soil aggregates may be larger than its minimal value. This simplification in DEAD scheme may cause the model to be overly prone to predict dust emission events and therefore increases emission frequency. In large scale global models, the sandblasting process (converting the horizontal sediment transport to vertical dust emissions) is also treated very simply. Here the DEAD scheme applies a globally uniform value to represent sandblasting, whereas observations and experiments show that soils with more fine particles tend to have larger sandblasting efficiencies. Ignoring the spatial heterogeneity in sandblasting efficiency reduces the modelled contribution of clay rich soils and, by contrast, amplifies the role of dust from bare land. In their fine scale global dust emission model, Chappell et al. (2023) reported much stronger seasonal variability of dust emissions in Australia than our results, mainly because their model implements the MB95 sandblasting parameterization using clay fraction data. Consequently, the difference in this parameterisation causes more dust emission flux in clay-rich regions and less where sediment has limited clay (North Africa and Middle East).

When computing u_{s*} in Eq. (7), we use 10 m wind speed as wind speed at freestream (U_f) following the same approach as LeGrand et al. (2023) implemented albedo-based sheltering in WRF-Chem. Other previous studies also use 10 m wind speed as U_f. However, as LeGrand et al. (2023) noted, the use of 10 m wind speed is not equivalent to the wind speed introduced by Chappell and Webb (2016) using Marshall's (1971) wind-tunnel experiments at freestream. The 10 m wind speed will be influenced differently by near-surface conditions to the wind speed at greater heights closer to freestream e.g., 40-100 m. Consequently, simulations using a standard 10 m height wind speed may introduce an additional source of bias into the albedo-based dust model that warrants further investigation.

5 Conclusion

The classical DEAD dust emission scheme as default in GEOS-Chem produces unrealistic spatial distributions of dust emission because of its simplified drag partition. To emulate the distribution of observed atmospheric dust requires the dust emission scheme to use a dust source function. In contrast, the DEAD scheme with a more sophisticated (albedo-based) drag partition and without a dust source function, produces a spatial distribution of dust emissions which compares well with atmospheric dust observations. This scheme performs as well as the classical dust models using the source function, indicating that the more detailed drag partition parameterization eliminates dust models' dependence on calibration to the spatial distribution of atmospheric dust observations.

Compared with results from the classical dust model using the source function, the albedo-based dust model produces similar spatial distribution and seasonality of dust emissions in barren land, but more emissions and pronounced seasonal variations in sparsely vegetated semi-arid regions. These differences are caused by classical dust models not representing the wind speed variations of the drag partition and their focus instead on representing the general trend of large-scale aerosol patterns. The

https://doi.org/10.5194/egusphere-2025-5872
Preprint. Discussion started: 4 February 2026

albedo-based dust model also makes a difference to the emission frequency, generating dust emissions with consistent seasonality in both total mass and frequency. Nevertheless, comparisons with observed atmospheric dust evaluate the albedo-based dust model for the first time, demonstrating it can simulate global atmospheric dust as well as classical models with a dust source function. Evidently, different patterns of dust emission frequency can produce similar atmospheric dust loadings, revealing that previous studies intent on reproducing general patterns of large-scale atmospheric dust burden have overlooked the equifinality of dust emission frequency.

We showed that the albedo-based dust model is straight-forward to implement in large scale dust models, requiring only one extra input variable from surface albedo data to provide dynamic roughness information for global dust models. Compared to classical dust modelling, the drag partition parameterization from satellite albedo observations, eliminates the dependency on source function and is able to represent the dynamic response of dust emissions to changes in land cover which are either slowly evolving (seasonality, invasive species) or abruptly changing (land use, wildfire and snow). However, accurate dust emission magnitude and frequency remain hampered by model parameterisation of entrainment threshold fixed over space, static over time with endless sediment supply, consistent with all other models.

6 Appendix A:

This appendix introduces the implementation of the albedo-based dust emission model within GEOS-Chem. It includes: (1) the modifications to the DEAD scheme required to introduce new input variables and functionality; (2) the workflow for computing and exporting MODIS-derived ω_{ns} fields in Google Earth Engine (GEE) and converting the outputs into NetCDF format compatible with GEOS-Chem; and (3) the run-time configuration updates needed to read the new inputs and generate online diagnostics of dust emissions.

A1 Integration of the albedo-based dust model into the DEAD scheme

Figure A1 shows the GEOS-Chem Classic file structure, including the source code tree and the run directory. The source code consists of the atmospheric chemistry component (GEOS-Chem) and the emission component (HEMCO). The HEMCO also maintains a separate run directory for standalone execution. All subroutines used for online emission calculations are contained within the HEMCO Extension, where the DEAD dust emission scheme is implemented in a file hcox_dead_mod.F.

All code modifications introduced in this study, including new variable declarations, initialization, assignment routines, computational algorithms, and memory de-allocation, are contained entirely within the DEAD scheme extension. Users wishing to enable the albedo-based dust emission model may simply replace the default hcox_dead_mod.F file with the modified version provided in the Code Availability section.

https://doi.org/10.5194/egusphere-2025-5872
Preprint. Discussion started: 4 February 2026

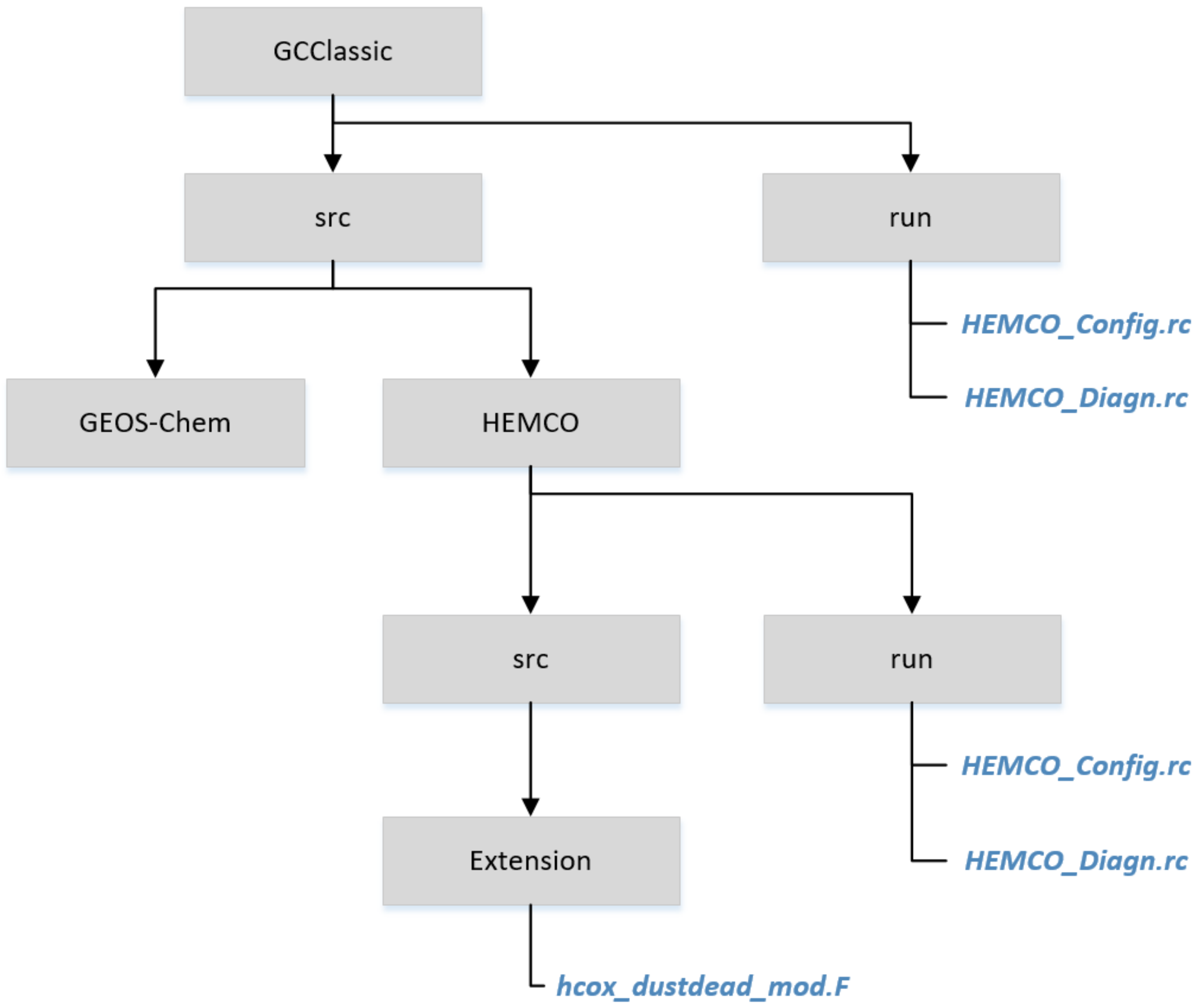

Figure A1. GEOS-Chem model architecture showing the directories and files referenced in this study. Directories are shown in boxes, and files are indicated in blue italics.

A2 Procuring and preprocessing MODIS-derived ω_{ns} data

We obtain the daily ω_{ns} fields using the Google Earth Engine (GEE, https://earthengine.google.com/). Band-1 black-sky albedo ($\omega_{dir}(0^{\circ})$) and the band-1 isotropic parameter (f_{iso}, rescaled by 0.001) from the 500 m MCD43A1 product were used to calculate ω_{ns} following Eq. (9) and Eq. (10) described in Section 2.1.2. All calculations were conducted at the native 500 m resolution and subsequently aggregated in GEE to 50 km resolution before being exported as GeoTIFF files. The full GEE script is provided in the Code Availability section.

https://doi.org/10.5194/egusphere-2025-5872
Preprint. Discussion started: 4 February 2026

The exported 50 km GeoTIFFs are then converted to daily GEOS-Chem-readable NetCDF files at 0.5° × 0.625° resolution using a Python script. The resulting NetCDF files follow GEOS-Chem conventions for temporal and spatial dimensions, coordinate conventions, variable definitions, and metadata, ensuring seamless ingestion by the model.

A3 modify the model run-time configuration file

The model run directory contains configuration files that specify extension switches, input/output paths, and variable names read by HEMCO. To enable the HEMCO extension to read the pre-processed ω_{ns} variable from NetCDF files, users must add the ω_{ns} input specification in the EXTENSION DATA section of HEMCO_Config.rc, providing the file path template, the temporal coverage and the variable name used in the NetCDF files. For example:

```
105 NS_ALBEDO    $ROOT/DUST_DEAD/NS_ALBEDO/$YYYY$MM$DD.nc    albedo  2016/1-12/1-31/0 C xy
unitless *  -  1 1
```

In addition, to enable diagnostic output of online dust emissions, users usually need to specify the diagnostic output path and variable names in HEMCO_Diagn.rc following:

```
InvDEAD_DST1   DST1  105  -1  -1  2  kg/m2/s  DST1_emission_flux_from_DEAD_extension
InvDEAD_DST2   DST2  105  -1  -1  2  kg/m2/s  DST2_emission_flux_from_DEAD_extension
InvDEAD_DST3   DST3  105  -1  -1  2  kg/m2/s  DST3_emission_flux_from_DEAD_extension
InvDEAD_DST4   DST4  105  -1  -1  2  kg/m2/s  DST4_emission_flux_from_DEAD_extension
```

For users who only require standalone dust emission calculation rather than atmospheric dust cycle simulation, analogous edits should be made to the standalone HEMCO configuration files. Example configuration files used in this study are provided in the Code Availability as reference templates.

Code and data availability. The GEOS-Chem v 14.2.3 source code is available in a Zenodo repository (https://zenodo.org/records/10246546, Yantosca et al., 2023). Our modified code, configuration files, and scripts for data processing are available at https://doi.org/10.6084/m9.figshare.30685316. The MODIS-Aqua dust aeroSol (MIDAS) observation dataset is available at https://doi.org/10.5281/zenodo.4244106 (Gkikas et al., 2021). The AERONET AOD observations are available at https://aeronet.gsfc.nasa.gov/ (Holben et al., 1998). Measured dust deposition flux and surface concentration are available at https://zenodo.org/records/6989502 (Li et al., 2022) and http://www.lisa.u-pec.fr/SDT/index.php?p=3 (Marticorena et al., 2010).

Author contributions. BL developed the model code, performed the simulations, and prepared the initial manuscript draft. HS conceived the study, designed the experiments, acquired funding, interpreted the results, and contributed to manuscript writing and revision. AC conceptualized the study and experiments and contributed to result interpretation and manuscript revision. ZZ contributed to model development, experimental design, and interpretation of the results.

Competing interests. The authors declare no conflicts of interest relevant to this study.

Acknowledgements. The authors acknowledge the Henan University for providing high-performance computing resources. This work was supported by the Natural Science Foundation of Henan Province, China (242300421143), the Technological Innovation Talents in Henan Higher Education Institutions of China (24HASTIT016), and the National Natural Science Foundation of China (32130066). The authors also acknowledge funding from the Faculty of Geographical Science and Engineering, Henan University, which enabled overseas exchange and study for the lead author at Cardiff University.

References:

Albani, S., Mahowald, N. M., Perry, A. T., Scanza, R. A., Zender, C. S., Heavens, N. G., Maggi, V., Kok, J. F., and Otto-Bliesner, B. L.: Improved dust representation in the Community Atmosphere Model, Journal of Advances in Modeling Earth Systems, 6, 541–570, https://doi.org/10.1002/2013MS000279, 2014.

AlNasser, F., Chehbouni, A., and Entekhabi, D.: Dust Source Areas and Their Plume Extent Derived From Satellite Data Fields, Geophysical Research Letters, 51, e2024GL110753, https://doi.org/10.1029/2024GL110753, 2024.

Anderson, T. L., Wu, Y., Chu, D. A., Schmid, B., Redemann, J., and Dubovik, O.: Testing the MODIS satellite retrieval of aerosol fine-mode fraction, Journal of Geophysical Research: Atmospheres, 110, https://doi.org/10.1029/2005JD005978, 2005.

Beven, K.: A manifesto for the equifinality thesis, Journal of Hydrology, 320, 18–36, https://doi.org/10.1016/j.jhydrol.2005.07.007, 2006.

Bey, I., Jacob, D. J., Yantosca, R. M., Logan, J. A., Field, B. D., Fiore, A. M., Li, Q., Liu, H. Y., Mickley, L. J., and Schultz, M. G.: Global modeling of tropospheric chemistry with assimilated meteorology: Model description and evaluation, Journal of Geophysical Research: Atmospheres, 106, 23073–23095, https://doi.org/10.1029/2001JD000807, 2001.

Cakmur, R. V., Miller, R. L., Perlwitz, J., Geogdzhayev, I. V., Ginoux, P., Koch, D., Kohfeld, K. E., Tegen, I., and Zender, C. S.: Constraining the magnitude of the global dust cycle by minimizing the difference between a model and observations, Journal of Geophysical Research: Atmospheres, 111, https://doi.org/10.1029/2005JD005791, 2006.

Chappell, A. and Webb, N. P.: Using albedo to reform wind erosion modelling, mapping and monitoring, Aeolian Research, 23, 63–78, https://doi.org/10.1016/j.aeolia.2016.09.006, 2016.

Chappell, A., Webb, N. P., Hennen, M., Zender, C. S., Ciais, P., Schepanski, K., Edwards, B. L., Ziegler, N. P., Balkanski, Y., Tong, D., Leys, J. F., Heidenreich, S., Hynes, R., Fuchs, D., Zeng, Z., Baddock, M. C., Lee, J. A., and Kandakji, T.: Elucidating Hidden and Enduring Weaknesses in Dust Emission Modeling, JGR Atmospheres, 128, e2023JD038584, https://doi.org/10.1029/2023JD038584, 2023a.

https://doi.org/10.5194/egusphere-2025-5872
Preprint. Discussion started: 4 February 2026

Chappell, A., Webb, N. P., Hennen, M., Schepanski, K., Ciais, P., Balkanski, Y., Zender, C. S., Tegen, I., Zeng, Z., Tong, D., Baker, B., Ekström, M., Baddock, M., Eckardt, F. D., Kandakji, T., Lee, J. A., Nobakht, M., von Holdt, J., and Leys, J. F.: Satellites reveal Earth's seasonally shifting dust emission sources, Science of the Total Environment, 883, https://doi.org/10.1016/j.scitotenv.2023.163452, 2023b.

Chappell, A., Hennen, M., Schepanski, K., Dhital, S., and Tong, D.: Reducing Resolution Dependency of Dust Emission Modeling Using Albedo-Based Wind Friction, Geophysical Research Letters, 51, e2023GL106540, https://doi.org/10.1029/2023GL106540, 2024.

Fairlie, T., Jacob, D. J., and Park, R. J.: The impact of transpacific transport of mineral dust in the United States, Atmospheric Environment, 41, 1251–1266, https://doi.org/10.1016/j.atmosenv.2006.09.048, 2007.

Friedl, M., and Sulla-Menashe, D.: MODIS/Terra+Aqua Land Cover Type Yearly L3 Global 0.05Deg CMG V061, NASA Land Processes Distributed Active Archive Center, https://doi.org/10.5067/MODIS/MCD12C1.061, 2022.

Ginoux, P., Chin, M., Tegen, I., Prospero, J. M., Holben, B., Dubovik, O., and Lin, S.-J.: Sources and distributions of dust aerosols simulated with the GOCART model, Journal of Geophysical Research: Atmospheres, 106, 20255–20273, https://doi.org/10.1029/2000JD000053, 2001.

Ginoux, P., Prospero, J., Torres, O., and Chin, M.: Long-term simulation of global dust distribution with the GOCART model: correlation with North Atlantic Oscillation, Environmental Modelling & Software, 19, 113–128, https://doi.org/10.1016/S1364-8152(03)00114-2, 2004.

Ginoux, P., Prospero, J. M., Gill, T. E., Hsu, N. C., and Zhao, M.: Global-scale attribution of anthropogenic and natural dust sources and their emission rates based on MODIS Deep Blue aerosol products, Reviews of Geophysics, 50, https://doi.org/10.1029/2012RG000388, 2012.

Gkikas, A., Proestakis, E., Amiridis, V., Kazadzis, S., Di Tomaso, E., Tsekeri, A., Marinou, E., Hatzianastassiou, N., and Pérez García-Pando, C.: ModIs Dust AeroSol (MIDAS): a global fine-resolution dust optical depth data set, Atmospheric Measurement Techniques, 14, 309–334, https://doi.org/10.5194/amt-14-309-2021, 2021.

Gómez Maqueo Anaya, S., Althausen, D., Faust, M., Baars, H., Heinold, B., Hofer, J., Tegen, I., Ansmann, A., Engelmann, R., Skupin, A., Heese, B., and Schepanski, K.: The implementation of dust mineralogy in COSMO5.05-MUSCAT, Geoscientific Model Development, 17, 1271–1295, https://doi.org/10.5194/gmd-17-1271-2024, 2024.

Hennen, M., Chappell, A., Webb, N. P., Schepanski, K., Baddock, M. C., Eckardt, F. D., Kandakji, T., Lee, J. A., Nobakht, M., and von Holdt, J.: A new framework for evaluating dust emission model development using dichotomous satellite observations of dust emission, Science of The Total Environment, 912, 169237, https://doi.org/10.1016/j.scitotenv.2023.169237, 2024.

Holben, B. N., Eck, T. F., Slutsker, I., Tanré, D., Buis, J. P., Setzer, A., Vermote, E., Reagan, J. A., Kaufman, Y. J., Nakajima, T., Lavenu, F., Jankowiak, I., and Smirnov, A.: AERONET—A Federated Instrument Network and Data Archive for Aerosol Characterization, Remote Sensing of Environment, 66, 1–16, https://doi.org/10.1016/S0034-4257(98)00031-5, 1998.

Huneeus, N., Schulz, M., Balkanski, Y., Griesfeller, J., Prospero, J., Kinne, S., Bauer, S., Boucher, O., Chin, M., Dentener, F., Diehl, T., Easter, R., Fillmore, D., Ghan, S., Ginoux, P., Grini, A., Horowitz, L., Koch, D., Krol, M. C., Landing, W., Liu, X., Mahowald, N., Miller, R., Morcrette, J.-J., Myhre, G., Penner, J., Perlwitz, J., Stier, P., Takemura, T., and Zender, C. S.: Global dust model intercomparison in AeroCom phase I, Atmospheric Chemistry and Physics, 11, 7781–7816, https://doi.org/10.5194/acp-11-7781-2011, 2011.

https://doi.org/10.5194/egusphere-2025-5872
Preprint. Discussion started: 4 February 2026

Johnson, M. S., Meskhidze, N., and Praju Kiliyanpilakkil, V.: A global comparison of GEOS-Chem-predicted and remotely-sensed mineral dust aerosol optical depth and extinction profiles, Journal of Advances in Modeling Earth Systems, 4, https://doi.org/10.1029/2011MS000109, 2012.

Kawamura, R.: Study on sand movement by wind, Tokyo Univ., Rep. Inst. Sc. Tech., 5, 95–112, 1951.

King, J., Nickling, W. G., and Gillies, J. A.: Representation of vegetation and other nonerodible elements in aeolian shear stress partitioning models for predicting transport threshold, J. Geophys. Res., 110, 2004JF000281, https://doi.org/10.1029/2004JF000281, 2005.

Klose, M., Jorba, O., Gonçalves Ageitos, M., Escribano, J., Dawson, M. L., Obiso, V., Di Tomaso, E., Basart, S., Montané Pinto, G., Macchia, F., Ginoux, P., Guerschman, J., Prigent, C., Huang, Y., Kok, J. F., Miller, R. L., and Pérez García-Pando, C.: Mineral dust cycle in the Multiscale Online Nonhydrostatic AtmospheRe CHemistry model (MONARCH) Version 2.0, Geoscientific Model Development, 14, 6403–6444, https://doi.org/10.5194/gmd-14-6403-2021, 2021.

Kok, J. F., Albani, S., Mahowald, N. M., and Ward, D. S.: An improved dust emission model – Part 2: Evaluation in the Community Earth System Model, with implications for the use of dust source functions, Atmospheric Chemistry and Physics, 14, 13043–13061, https://doi.org/10.5194/acp-14-13043-2014, 2014.

Kok, J. F., Adebiyi, A. A., Albani, S., Balkanski, Y., Checa-Garcia, R., Chin, M., Colarco, P. R., Hamilton, D. S., Huang, Y., Ito, A., Klose, M., Leung, D. M., Li, L., Mahowald, N. M., Miller, R. L., Obiso, V., Pérez García-Pando, C., Rocha-Lima, A., Wan, J. S., and Whicker, C. A.: Improved representation of the global dust cycle using observational constraints on dust properties and abundance, Atmospheric Chemistry and Physics, 21, 8127–8167, https://doi.org/10.5194/acp-21-8127-2021, 2021.

Ku, B. and Park, R. J.: Comparative inverse analysis of satellite (MODIS) and ground (PM10) observations to estimate dust emissions in East Asia, Asia-Pacific J Atmos Sci, 49, 3–17, https://doi.org/10.1007/s13143-013-0002-5, 2013.

LeGrand, S. L., Letcher, T. W., Okin, G. S., Webb, N. P., Gallagher, A. R., Dhital, S., Hodgdon, T. S., Ziegler, N. P., and Michaels, M. L.: Application of a satellite-retrieved sheltering parameterization (v1.0) for dust event simulation with WRF-Chem v4.1, Geoscientific Model Development, 16, 1009–1038, https://doi.org/10.5194/gmd-16-1009-2023, 2023.

Leung, D. M., Kok, J. F., Li, L., Okin, G. S., Prigent, C., Klose, M., Pérez García-Pando, C., Menut, L., Mahowald, N. M., Lawrence, D. M., and Chamecki, M.: A new process-based and scale-aware desert dust emission scheme for global climate models – Part I: Description and evaluation against inverse modeling emissions, Atmospheric Chemistry and Physics, 23, 6487–6523, https://doi.org/10.5194/acp-23-6487-2023, 2023.

Li, L., Mahowald, N. M., Kok, J. F., Liu, X., Wu, M., Leung, D. M., Hamilton, D. S., Emmons, L. K., Huang, Y., Sexton, N., Meng, J., and Wan, J.: Importance of different parameterization changes for the updated dust cycle modeling in the Community Atmosphere Model (version 6.1), Geoscientific Model Development, 15, 8181–8219, https://doi.org/10.5194/gmd-15-8181-2022, 2022.

Mahowald, N. M., Muhs, D. R., Levis, S., Rasch, P. J., Yoshioka, M., Zender, C. S., and Luo, C.: Change in atmospheric mineral aerosols in response to climate: Last glacial period, preindustrial, modern, and doubled carbon dioxide climates, Journal of Geophysical Research: Atmospheres, 111, https://doi.org/10.1029/2005JD006653, 2006.

Mahowald, N. M., Engelstaedter, S., Luo, C., Sealy, A., Artaxo, P., Benitez-Nelson, C., Bonnet, S., Chen, Y., Chuang, P. Y., Cohen, D. D., Dulac, F., Herut, B., Johansen, A. M., Kubilay, N., Losno, R., Maenhaut, W., Paytan, A., Prospero, J. M., Shank, L. M., and Siefert, R. L.: Atmospheric Iron Deposition: Global Distribution, Variability, and Human Perturbations*, Annual Review of Marine Science, 1, 245–278, https://doi.org/10.1146/annurev.marine.010908.163727, 2009.

https://doi.org/10.5194/egusphere-2025-5872
Preprint. Discussion started: 4 February 2026

Marshall, J. K.: Drag measurements in roughness arrays of varying density and distribution, Agricultural Meteorology, 8, 269–292, https://doi.org/10.1016/0002-1571(71)90116-6, 1971.

Marticorena, B. and Bergametti, G.: Modeling the atmospheric dust cycle: 1. Design of a soil-derived dust emission scheme, Journal of Geophysical Research: Atmospheres, 100, 16415–16430, https://doi.org/10.1029/95JD00690, 1995.

Marticorena, B., Chatenet, B., Rajot, J. L., Traoré, S., Coulibaly, M., Diallo, A., Koné, I., Maman, A., NDiaye, T., and Zakou, A.: Temporal variability of mineral dust concentrations over West Africa: analyses of a pluriannual monitoring from the AMMA Sahelian Dust Transect, Atmospheric Chemistry and Physics, 10, 8899–8915, https://doi.org/10.5194/acp-10-8899-2010, 2010.

Mayaud, J. R. and Webb, N. P.: Vegetation in Drylands: Effects on Wind Flow and Aeolian Sediment Transport, Land, 6, 64, https://doi.org/10.3390/land6030064, 2017.

Meng, J., Martin, R. V., Ginoux, P., Hammer, M., Sulprizio, M. P., Ridley, D. A., and van Donkelaar, A.: Grid-independent high-resolution dust emissions (v1.0) for chemical transport models: application to GEOS-Chem (12.5.0), Geoscientific Model Development, 14, 4249–4260, https://doi.org/10.5194/gmd-14-4249-2021, 2021.

Okin, G. S.: A new model of wind erosion in the presence of vegetation, J. Geophys. Res., 113, 2007JF000758, https://doi.org/10.1029/2007JF000758, 2008.

Prospero, J. M.: The atmospheric transport of particles to the ocean, in: Particle Flux in the Ocean, edited by: Ittekkot, V., Schaefer, P., Honjo, S., and Depetris, P. J., John Wiley and Sons, Hoboken, 19–52, 1996.

Prospero, J. M., Ginoux, P., Torres, O., Nicholson, S. E., and Gill, T. E.: Environmental Characterization of Global Sources of Atmospheric Soil Dust Identified with the Nimbus 7 Total Ozone Mapping Spectrometer (toms) Absorbing Aerosol Product, Reviews of Geophysics, 40, 2-1-2–31, https://doi.org/10.1029/2000RG000095, 2002.

Raupach, M. and Lu, H.: Representation of land-surface processes in aeolian transport models, Environmental Modelling & Software, 19, 93–112, https://doi.org/10.1016/S1364-8152(03)00113-0, 2004.

Raupach, M. R.: Drag and drag partition on rough surfaces, Boundary-Layer Meteorol, 60, 375–395, https://doi.org/10.1007/BF00155203, 1992.

Raupach, M. R., Gillette, D. A., and Leys, J. F.: The effect of roughness elements on wind erosion threshold, Journal of Geophysical Research: Atmospheres, 98, 3023–3029, https://doi.org/10.1029/92JD01922, 1993.

Ridley, D. A., Heald, C. L., Pierce, J. R., and Evans, M. J.: Toward resolution-independent dust emissions in global models: Impacts on the seasonal and spatial distribution of dust, Geophysical Research Letters, 40, 2873–2877, https://doi.org/10.1002/grl.50409, 2013.

Shao, Y., Nickling, W., Bergametti, G., Butler, H., Chappell, A., Findlater, P., Gillies, J., Ishizuka, M., Klose, M., Kok, J. F., Leys, J., Lu, H., Marticorena, B., McTainsh, G., McKenna-Neuman, C., Okin, G. S., Strong, C., and Webb, N.: A tribute to Michael R. Raupach for contributions to aeolian fluid dynamics, Aeolian Research, 19, 37–54, https://doi.org/10.1016/j.aeolia.2015.09.004, 2015.

Shao, Y., Chen, S., Huang, N., Gui, H., Mao, R., Masahide, I., Wu, C., Yin, X., and Zhang, J.: Source Limitation Could Have Major Implications to Dust Emission Estimates, Geophysical Research Letters, 52, e2024GL112562, https://doi.org/10.1029/2024GL112562, 2025.

https://doi.org/10.5194/egusphere-2025-5872
Preprint. Discussion started: 4 February 2026

Sherman, D. J., Li, B., Ellis, J. T., Farrell, E. J., Maia, L. P., and Granja, H.: Recalibrating aeolian sand transport models, Earth Surface Processes and Landforms, 38, 169–178, https://doi.org/10.1002/esp.3310, 2013.

Shinoda, M., Gillies, J. A., Mikami, M., and Shao, Y.: Temperate grasslands as a dust source: Knowledge, uncertainties, and challenges, Aeolian Research, 3, 271–293, https://doi.org/10.1016/j.aeolia.2011.07.001, 2011.

Singh, I., Martin, R. V., Bindle, L., Chatterjee, D., Li, C., Oxford, C., Xu, X., and Wang, J.: Effect of Dust Morphology on Aerosol Optics in the GEOS-Chem Chemical Transport Model, on UV-Vis Trace Gas Retrievals, and on Surface Area Available for Reactive Uptake, Journal of Advances in Modeling Earth Systems, 16, e2023MS003746, https://doi.org/10.1029/2023MS003746, 2024.

Song, H., Min, R., Song, G., Zhai, S., Wang, D., Wang, Y., and Bai, T.: Impacts of land cover changes on dust emissions in northern China (2000–2020), Land Degradation & Development, 35, 2800–2812, https://doi.org/10.1002/ldr.5094, 2024.

Tanaka, T. Y. and Chiba, M.: A numerical study of the contributions of dust source regions to the global dust budget, Global and Planetary Change, 52, 88–104, https://doi.org/10.1016/j.gloplacha.2006.02.002, 2006.

Taylor, K. E.: Summarizing multiple aspects of model performance in a single diagram, Journal of Geophysical Research: Atmospheres, 106, 7183–7192, https://doi.org/10.1029/2000JD900719, 2001.

Tegen, I., Harrison, S. P., Kohfeld, K., Prentice, I. C., Coe, M., and Heimann, M.: Impact of vegetation and preferential source areas on global dust aerosol: Results from a model study, J. Geophys. Res., 107, https://doi.org/10.1029/2001JD000963, 2002.

Tian, R., Ma, X., and Zhao, J.: A revised mineral dust emission scheme in GEOS-Chem: improvements in dust simulations over China, Atmospheric Chemistry and Physics, 21, 4319–4337, https://doi.org/10.5194/acp-21-4319-2021, 2021.

Walling, D. E.: Assessing the accuracy of suspended sediment rating curves for a small basin, Water Resources Research, 13, 531–538, https://doi.org/10.1029/WR013i003p00531, 1977.

Webb, N. P., Okin, G. S., and Brown, S.: The effect of roughness elements on wind erosion: The importance of surface shear stress distribution, JGR Atmospheres, 119, 6066–6084, https://doi.org/10.1002/2014JD021491, 2014.

Webb, N. P., Herrick, J. E., Van Zee, J. W., Courtright, E. M., Hugenholtz, C. H., Zobeck, T. M., Okin, G. S., Barchyn, T. E., Billings, B. J., Boyd, R., Clingan, S. D., Cooper, B. F., Duniway, M. C., Derner, J. D., Fox, F. A., Havstad, K. M., Heilman, P., LaPlante, V., Ludwig, N. A., Metz, L. J., Nearing, M. A., Norfleet, M. L., Pierson, F. B., Sanderson, M. A., Sharratt, B. S., Steiner, J. L., Tatarko, J., Tedela, N. H., Toledo, D., Unnasch, R. S., Van Pelt, R. S., and Wagner, L.: The National Wind Erosion Research Network: Building a standardized long-term data resource for aeolian research, modeling and land management, Aeolian Research, 22, 23–36, https://doi.org/10.1016/j.aeolia.2016.05.005, 2016.

Webb, N. P., Chappell, A., LeGrand, S. L., Ziegler, N. P., and Edwards, B. L.: A note on the use of drag partition in aeolian transport models, Aeolian Research, 42, 100560, https://doi.org/10.1016/j.aeolia.2019.100560, 2020.

White, B. R.: soil transport by winds on Mars, Journal of Geophysical Research: Solid Earth, 84, 4643–4651, https://doi.org/10.1029/JB084iB09p04643, 1979.

Wu, C., Lin, Z., Liu, X., Ji, D., Zhang, H., Li, C., and Lin, G.: Description of Dust Emission Parameterization in CAS-ESM2 and Its Simulation of Global Dust Cycle and East Asian Dust Events, Journal of Advances in Modeling Earth Systems, 13, e2020MS002456, https://doi.org/10.1029/2020MS002456, 2021.

https://doi.org/10.5194/egusphere-2025-5872
Preprint. Discussion started: 4 February 2026

Yantosca, B., Sulprizio, M., Lundgren, L., Keller, C., kelvinhb, Fritz, T., Lin, H., 22degrees, Ridley, D., Bindle, L., michael-s-long, Eastham, S. D., tsherwen, Downs, W., Fisher, J., Thackray, C., Holmes, C., GanLuo, Zhuang, J., Murray, L., SpaceMouse, Estrada, L. A., Shutter, J., noelleselin, Long, M., nicholasbalasus, xin-chen-github, emily-ramnarine, gianga, and Haskins, D. J.: geoschem/geos-chem: GEOS-Chem (science codebase) 14.2.3, , https://doi.org/10.5281/zenodo.10246546, 2023.

Zender, C. S., Bian, H., and Newman, D.: Mineral Dust Entrainment and Deposition (DEAD) model: Description and 1990s dust climatology, Journal of Geophysical Research: Atmospheres, 108, https://doi.org/10.1029/2002JD002775, 2003.

Zhang, L., Kok, J. F., Henze, D. K., Li, Q., and Zhao, C.: Improving simulations of fine dust surface concentrations over the western United States by optimizing the particle size distribution, Geophysical Research Letters, 40, 3270–3275, https://doi.org/10.1002/grl.50591, 2013.

Zhou, Z., Zhang, C., Chappell, A., Zou, X., Zhang, Z., Zuo, X., Zhang, X., Zhou, J., and Cao, Z.: Using Field Measurements Across Land Cover Types to Evaluate Albedo-Based Wind Friction Velocity and Estimate Sediment Transport, Journal of Geophysical Research: Atmospheres, 129, e2023JD040313, https://doi.org/10.1029/2023JD040313, 2024.

Zuidema, P., Alvarez, C., Kramer, S. J., Custals, L., Izaguirre, M., Sealy, P., Prospero, J. M., and Blades, E.: Is Summer African Dust Arriving Earlier to Barbados? The Updated Long-Term In Situ Dust Mass Concentration Time Series from Ragged Point, Barbados, and Miami, Florida, Bull. Am. Meteorol. Soc., 100, 1981–1986, https://doi.org/10.1175/BAMS-D-18-0083.1, 2019.